Anomalous couplings in double Higgs production

Author(s):
Contino, Roberto; Ghezzi, Margherita; Moretti, Mauro; Panico, Giuliano; Piccinini, Fulvio; Wulzer, Andrea

Anomalous couplings in double Higgs production

Roberto Contino,[a] **Margherita Ghezzi,**[a] **Mauro Moretti,**[b] **Giuliano Panico,**[c]
Fulvio Piccinini[d] **and Andrea Wulzer**[c,e]

[a] *Dipartimento di Fisica, Università di Roma "La Sapienza" and INFN — Sezione di Roma,*
Roma, Italy

[b] *Dipartimento di Fisica, Università di Ferrara and INFN — Sezione di Ferrara,*
Ferrara, Italy

[c] *Institute for Theoretical Physics, ETH,*
CH-8093, Zurich, Switzerland

[d] *INFN — Sezione di Pavia,*
Pavia, Italy

[e] *Dipartimento di Fisica e Astronomia and INFN — Sezione di Padova,*
Padova, Italy

E-mail: roberto.contino@roma1.infn.it,
Margherita.Ghezzi@roma1.infn.it, moretti@fe.infn.it,
panico@phys.ethz.ch, Fulvio.Piccinini@pv.infn.it, wulzer@pd.infn.it

ABSTRACT: The process of gluon-initiated double Higgs production is sensitive to non-linear interactions of the Higgs boson. In the context of the Standard Model, studies of this process focused on the extraction of the Higgs trilinear coupling. In a general parametrization of New Physics effects, however, an even more interesting interaction that can be tested through this channel is the $t\bar{t}hh$ coupling. This interaction vanishes in the Standard Model and is a genuine signature of theories in which the Higgs boson emerges from a strongly-interacting sector. In this paper we perform a model-independent estimate of the LHC potential to detect anomalous Higgs couplings in gluon-fusion double Higgs production. We find that while the sensitivity to the trilinear is poor, the perspectives of measuring the new $t\bar{t}hh$ coupling are rather promising.

Contents

1 Introduction

Measuring the couplings of the Higgs boson at the LHC is a difficult but important task. It will give crucial information to distinguish among different theoretical scenarios that can lead to a Higgs-like particle, and can thus shed light on the mechanism behind electroweak symmetry breaking (EWSB). In the Standard Model (SM), the request of perturbativity and unitarity up to Planckian scales fixes the strength of all the interactions of the Higgs boson in terms of its mass. Sizable modifications of the couplings can arise in weakly-coupled extensions, such as supersymmetry, through the mixing of the Higgs boson with new light states. In this case one expects to produce these new particles directly at the collider. A second compelling possibility is that the EWSB is triggered by new strong dynamics at the TeV scale, and a light Higgs emerges as the pseudo Nambu-Goldstone boson (pNGB) of a larger spontaneously broken symmetry [1–7]. In this case the modification of couplings is not necessarily accompanied by the presence of new light scalars and the direct manifestation of New Physics can be postponed to TeV energies. In addition to a modified pattern of linear couplings, this scenario predicts new non-linear interactions of the Higgs to the SM fields, which can lead to striking signatures at the collider and are a genuine feature of the underlying strong dynamics.

The problem of extracting the Higgs couplings by measuring its production and decay rates at the LHC has been studied at length in the literature, see for example refs. [8–15]. The importance of a model-independent approach has been recently re-discussed, and a first estimate of the impact of the current LHC data on the Higgs parameter space has been performed in [16–25].

Aim of this paper is to study the effect of anomalous couplings in the process of gluon-initiated double Higgs production at the LHC, $gg \to hh$. Under the reasonable assumption

of weak couplings to light fermions, this process proceeds through top quark loops and it is thus sensitive, in the first place, to the Higgs-top couplings. It also receives a contribution from the Higgs trilinear coupling, and for this reason has been studied in detail in the context of the SM [26–32]. In theories of New Physics, however, a much more interesting coupling that can be probed through this process is the non-linear interaction $t\bar{t}hh$. The latter is generally present in theories of composite Higgs, like for example the minimal models MCHM4 [33] and MCHM5 [34], and gives a genuine signal of the Higgs strong interactions. As first noticed by the authors of ref. [35] (see also ref. [36] for a discussion of the role of the $t\bar{t}hh$ coupling in context of Little Higgs theories), the presence of the new coupling can lead to a dramatic increase of the cross section. For example, enhancements larger than one order of magnitude are possible in the MCHM5, and even for $(v/f)^2 \sim 0.15$, where f is the decay constant of the pNGB Higgs, the total cross section *doubles* compared to its SM value. Given that the deviations due to Higgs compositeness are usually much milder, $gg \to hh$ seems an extremely favored channel which is worth investigating.

In this paper we derive a first quantitative assessment on the detectability of the anomalous coupling $t\bar{t}hh$ in the process $gg \to hh$. We do not consider the rarer process of double-Higgs production via vector boson fusion, which has been investigated at the LHC in previous studies [37–40], since it is sensitive to the couplings of the Higgs to vector bosons and to the Higgs trilinear coupling. Neglecting such process is a very good approximation, considering that in absence of dedicated kinematic cuts its rate at the LHC is much smaller than the rate of $gg \to hh$. In section 2 we briefly summarize the parametrization of the couplings of a generic Higgs-like scalar which we adopt. In section 3 we analyze the $gg \to hh$ process in the presence of modified Higgs interactions. In particular we study the dependence of the cross section on the various couplings and show that there is high sensitivity to the new $t\bar{t}hh$ coupling, much larger than that on the trilinear self-interaction. For our analysis we wrote a dedicated computer code which computes the exact 1-loop matrix element for single and double Higgs production via gluon fusion as a function of the relevant couplings. The code has been implemented as one of the available processes of the event generator ALPGEN [41] and will be made public with its next official release. We then discuss two of the most promising decay channels of the Higgs pair: $hh \to WW\gamma\gamma \to l\nu j j\gamma\gamma$ in the case in which the Higgs has a suppressed single coupling to the top (fermiophobic limit), and $hh \to b\bar{b}\gamma\gamma$ in the case in which the linear couplings are SM like. For the latter case, we follow the strategy proposed in ref. [32] and in section 4 we perform a first collider study to estimate the exclusion and discovery limits on the anomalous $t\bar{t}hh$ coupling. To compute the SM background cross section we use the results of [32] with updated b and γ efficiencies and rejection factors. We collect the results of our collider study in section 4.1. Finally, conclusions are reported in section 5.

2   General parametrization of the Higgs couplings

In this section we introduce the general parametrization of Higgs couplings that will be used in this paper.

The most general effective Lagrangian that parametrizes the interactions of a Higgs-like scalar at low energy has been discussed in [39] and extended in [17]. Under the assumption of custodial symmetry, the Nambu-Goldstone bosons associated to the electroweak symmetry breaking can be described as the coordinates of the coset $SU(2)_L \times SU(2)_R / SU(2)_V \sim SO(4)/SO(3)$. They can be conveniently parametrized by the 2×2 matrix

$$\Sigma = \exp\left(i\sigma_a \chi^a(x)/v\right), \qquad a = 1, 2, 3 \tag{2.1}$$

where σ^a are the Pauli matrices and $v = 246$ GeV. At energy scales much below possible new physics states, the effective Lagrangian describing a light Higgs h has the form

$$\mathcal{L} = \frac{v^2}{4} \text{Tr}(D_\mu \Sigma^\dagger D^\mu \Sigma) \left(1 + 2a\frac{h}{v} + \ldots\right) + \frac{1}{2}(\partial_\mu h)^2 - \frac{1}{2}m_h^2 h^2 - d_3 \frac{1}{6}\left(\frac{3m_h^2}{v}\right)h^3 + \ldots$$
$$- m_t\, \bar{q}_L^i \Sigma_{i1} t_R \left(1 + c_t\frac{h}{v} + c_2\frac{h^2}{v^2} + \ldots\right) - m_b\, \bar{q}_L^i \Sigma_{i2} b_R \left(1 + c_b\frac{h}{v} + \ldots\right) + \text{h.c.}, \tag{2.2}$$

where $q_L = (t_L, b_L)$ and a, $c_{t,b}$, c_2 and d_3 are the numerical coefficients that parametrize the Higgs couplings. The dots stand for terms which are not relevant for double Higgs production via gluon-fusion. In particular, we assume that the strength of single interactions of the Higgs to the fermions is not extremely enhanced compared to its SM value, so that the contribution of the light fermions and the bottom quark to double Higgs production can be safely neglected. The coupling to the bottom, c_b, is relevant only in the Higgs decay, and we will set

$$c_t = c_b = c \tag{2.3}$$

for simplicity in the following. We also neglect ggh and $gghh$ local interactions which can be generated by new heavy states at 1-loop level, as for example scalar or fermionic partners of the top quark (see ref. [42] for a study of the effect of such local interactions).

In this analysis we will freely vary the parameters that appear in the effective Lagrangian. In specific models, however, they can be related to each other. For example, the SM Lagrangian is obtained for

$$a = c = d_3 = 1, \qquad c_2 = 0. \tag{2.4}$$

A class of theories that we will consider in the following are the composite Higgs models based on the symmetry pattern $SO(5)/SO(4)$ [33, 34]. In these models the parameter a is given by

$$a = \sqrt{1 - \xi}, \tag{2.5}$$

where $\xi = v^2/f^2$ and f is the Nambu-Goldstone decay constant. The values of c, c_2 and d_3 depend on which $SO(5)$ representation the fermions are embedded in. For the two minimal choices of fermions in the spinorial (MCHM4 [33]) and fundamental (MCHM5 [34])
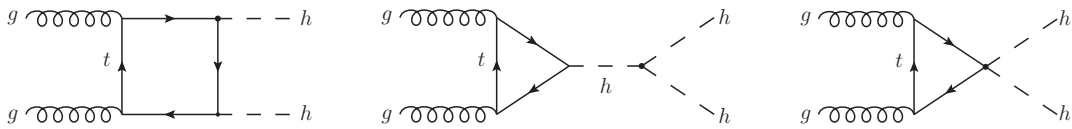
Figure 1. Feynman diagrams for double Higgs production via gluon fusion (an additional contribution comes from the crossing of the box diagram). The last diagram contains the new non-linear Higgs interaction $t\bar{t}hh$.

representations one gets

$$c = d_3 = \sqrt{1-\xi}\,, \qquad c_2 = -\frac{\xi}{2}\,, \qquad \text{MCHM4, spinorial representation}\,, \qquad (2.6)$$

$$c = d_3 = \frac{1-2\xi}{\sqrt{1-\xi}}\,, \qquad c_2 = -2\xi\,, \qquad \text{MCHM5, fundamental representation}\,. \quad (2.7)$$

Equations (2.5), (2.6) and (2.7) account for the value of the Higgs couplings as due to the non-linearities of the chiral Lagrangian. The exchange of new heavy particles can however give further corrections to these expressions. In the following we will neglect these effects since they are parametrically subleading [43], although they can be numerically important when the top or bottom degree of compositeness becomes large [44]. This is especially justified considering that in minimal composite Higgs models with partial compositeness these additional corrections to the couplings do not affect the $gg \to h$ rate because they are exactly canceled by the contribution from loops of heavy fermions, as first observed in refs. [43, 45, 46] and explained in ref. [44]. For double Higgs production we expect this cancellation to occur only in the limit of vanishing momentum of the Higgs external lines. In general, numerically important contributions might come from light top partners (light custodians). In models with partial compositeness, where the dominant contribution to the Higgs potential comes from top loops, the presence of light fermionic resonances is essential to obtain a light Higgs [34, 47–51]. In particular, $m_h \simeq 120 - 130$ GeV requires top partners around or below 1 TeV. It would be interesting to analyze in detail their effects on double Higgs production.

3   Double Higgs production via gluon fusion

In the scenario we are considering, the leading-order contributions to the process $gg \to hh$ come from Feynman diagrams containing a top-quark loop. The three relevant diagrams are shown in figure 1, and can be computed by using the results of ref. [27]. We have implemented the automatic computation of the matrix element as one of the processes of the ALPGEN MonteCarlo generator [41]. The code will be made public with the next official release of ALPGEN, and it allows one to compute the total cross section and differential distributions, as well as to generate events for an arbitrary choice of the Higgs couplings c, d_3, c_2. The validation of the code has been performed by means of an independent C++ program linked to the QCDLoop [52] and to the LHAPDF routines [53]. All the results reported in the following have been derived by use of the ALPGEN matrix element calcu-
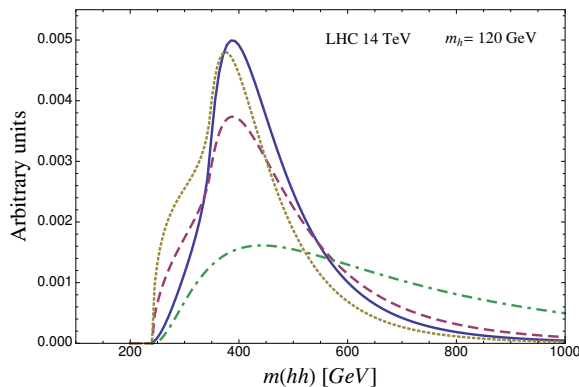
Figure 2. Invariant mass distribution of the two Higgs bosons in $pp \to hh$ at the LHC (14 TeV) for $m_h = 120$ GeV. The various curves correspond to different choices of Higgs couplings: $c = d_3 = 1$, $c_2 = 0$ (SM couplings, solid blue curve), $c = d_3 = 1$, $c_2 = -1$ (dashed purple curve), $c = 1$, $d_3 = c_2 = 0$ (dotted yellow curve). The dot-dashed green curve shows the distribution obtained in the approximation of infinite top mass with SM couplings. All curves have been normalized to unit area. The corresponding LO total cross sections are 15.2 fb (solid blue curve), 253 fb (dashed purple curve), 31.6 fb (dotted yellow curve).

lation with CTEQ6l parton distribution functions and renormalization and factorization scales $Q = m(hh)$. The top quark mass has been set to $m_t = 173$ GeV.

The amplitude of each diagram in figure 1 is characterized by a different energy scaling at large invariant masses $\sqrt{\hat{s}} = m(hh) \gg m_t, m_h$. One has

$$\mathcal{A}_\square \sim c^2 \, \alpha_s \frac{m_t^2}{v^2} \, , \tag{3.1}$$

$$\mathcal{A}_\triangle \sim c \, d_3 \, \alpha_s \frac{m_t^2}{v^2} \, \frac{m_h^2}{\hat{s}} \left[\log\left(\frac{m_t^2}{\hat{s}}\right) + i\pi \right]^2 \, , \tag{3.2}$$

$$\mathcal{A}_{\triangle nl} \sim c_2 \, \alpha_s \frac{m_t^2}{v^2} \left[\log\left(\frac{m_t^2}{\hat{s}}\right) + i\pi \right]^2 \, , \tag{3.3}$$

where $\mathcal{A}_\square$, $\mathcal{A}_\triangle$ are the amplitudes of respectively the box and the triangle diagram with the Higgs exchange (first two diagrams of figure 1), while $\mathcal{A}_{\triangle nl}$ denotes the amplitude of the diagram with the new non-linear interaction $t\bar{t}hh$ (last diagram of figure 1). At large $\hat{s}$ the box and the diagram with the new vertex dominate, while the triangle with Higgs exchange gives its largest contribution near threshold. For SM values of the couplings there is a destructive interference between $\mathcal{A}_\triangle$ and $\mathcal{A}_\square$, so that decreasing the trilinear coupling d_3 leads to a softer distribution, while increasing it makes the suppression of the cross section near threshold even stronger. On the other hand, since $\mathcal{A}_{\triangle nl}$ and $\mathcal{A}_\square$ have similar energy scalings (the log enhancement of $\mathcal{A}_{\triangle nl}$ becomes important only at very large $\sqrt{\hat{s}}$ where the gluon pdfs are small), the main effect of their interference is on the total cross section, with little modification of the $m(hh)$ distribution. These behaviours are clearly visible in the distributions shown in figure 2 for $m_h = 120$ GeV at 14 TeV.

The cross section depends on the couplings as a quadratic polynomial in the variables c_2, c^2 and cd_3, associated respectively to the three diagrams of figure 1. It can thus be

		$\overline{\sigma}$	α	β	A_1	A_2	A_3
$m_h =$ 120 GeV	14 TeV	151.3 fb	0.453	0.164	-1.86	-1.77	1.66
	8 TeV	32.6 fb	0.474	0.178	-1.89	-1.78	1.68
$m_h =$ 125 GeV	14 TeV	144.6 fb	0.457	0.169	-1.85	-1.79	1.68
	8 TeV	30.5 fb	0.475	0.185	-1.89	-1.79	1.70

Table 1. Coefficients for the fit of eq. (3.4) of the total LO $pp \to hh$ cross section via gluon fusion at the LHC.

conveniently expressed by the formula

$$\sigma(pp \to hh) = \overline{\sigma} \left[c_2^2 + \left(\alpha\, c^2 \right)^2 + (\beta\, cd_3)^2 + A_1\, c_2 \left(\alpha\, c^2 \right) + A_2 \left(\alpha\, c^2 \right) (\beta\, cd_3) + A_3\, c_2 \left(\beta\, cd_3 \right) \right] , \tag{3.4}$$

where the value of the (real) coefficients $\overline{\sigma}, \alpha, \beta, A_1, A_2, A_3$ has been extracted by fitting the results of a MonteCarlo integration, and is reported in table 1 (at LO in α_s) for $m_h = 120, 125$ GeV at 8 and 14 TeV. In the above parametrization, the coefficients α and β measure the sensitivity of the cross section on the parameters c^2 and (cd_3), relative to c_2. One can see from table 1 that the dependence on c^2 is significant while the one on (cd_3) is rather mild. This can be tracked back to the additional factor $(m_h^2/\hat{s})$ in the amplitude of the triangle diagram which carries the dependence on (cd_3), see eq. (3.2). This factor leads to a suppression at large $\hat{s}$ and thus, because of the kinematic threshold $\hat{s} > 4m_h^2$, to a reduction of the sensitivity on (cd_3) of the total cross section.

We see in table 1 that increasing the LHC center-of-mass energy from 8 TeV to 14 TeV increases the LO total cross section (hence the coefficient $\bar{\sigma}$) by a factor ~ 5.2, while the relative strength among $\alpha, \beta, A_1, A_2, A_3$ varies by less than $\sim 15\%$. When the Higgs mass is varied from 120 GeV to 125 GeV, $\bar{\sigma}$ decreases by $\sim 5 - 7\%$, while the other coefficients change by less than $\sim 1 - 3\%$. The left plot of figure 3 illustrates how the total cross section changes when varying individually d_3 and c_2, while fixing the other couplings to their SM value. In the vicinity of the SM point, decreasing (increasing) d_3 or c_2 leads to an enhancement (reduction) of the total cross section, with a much stronger dependence on c_2 than on d_3. The right plot in the same figure shows how the cross section varies with the Higgs mass for the SM choice of couplings. The solid curve corresponds to the full one-loop matrix element calculation, while the dot-dashed curve is obtained by taking the limit of infinite top mass. As previously noticed [29],[1] this approximation is reasonably accurate in the case of the total cross section, but completely fails to reproduce the correct $m(hh)$ distribution, as illustrated by the corresponding curve in figure 2.

We have seen that modified Higgs couplings, in particular a non-vanishing $t\bar{t}hh$ interaction, can lead to a strong enhancement of the total $pp \to hh$ cross section. However, in order to determine the signal yield at the LHC in a given final state one has to take into account also the change in the Higgs decay branching ratios. In our case, these latter

---

[1]The infinite top mass limit is also discussed by the authors of ref. [26], although the contribution of the triangle diagram seems to have been accidentally omitted in their figure 2.
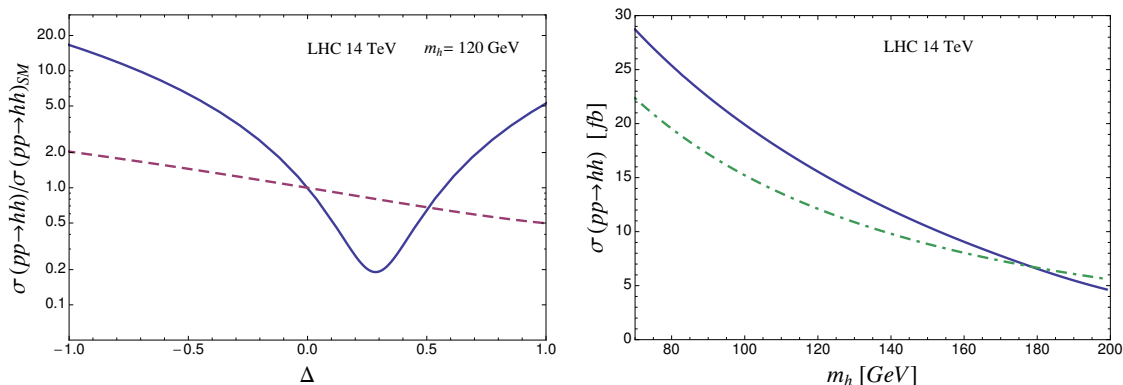
Figure 3. Left plot: total cross section in SM units as a function of $c_2 = \Delta$ (solid blue curve) and $d_3 = 1 + \Delta$ (dashed purple curve), with the other Higgs couplings set to their SM values and $m_h = 120\,\text{GeV}$. Right plot: LO total cross section (in fb) in the SM as a function of m_h as computed by means of the full one-loop matrix element (solid blue curve) and the infinite top mass approximation (dot-dashed green curve). In both plots the LHC center-of-mass energy has been set to $14\,\text{TeV}$.

depend only on the ratio of the parameters c and a. We will consider two illustrative situations: *i)* the case in which the branching ratios are similar to the SM ones; *ii)* the case in which the couplings of one Higgs boson to two fermions are suppressed (fermiophobic limit). The first situation is realized in models where all single Higgs couplings are rescaled by the same factor (as in the MCHM4, see eqs. (2.5), (2.6)), or their shift from the SM value is small (as in composite Higgs models with small ξ). In this case the studies of refs. [29–32] suggest that the most favorable final state at the LHC for a light Higgs boson is $hh \to \gamma\gamma b\bar{b}$. On the other hand, if single Higgs couplings to fermions are suppressed (while the strength of $t\bar{t}hh$ can still be sizable), the dominant decay mode for a light Higgs becomes $h \to WW$. The channel $hh \to WWWW$ has in this case the largest rate and should be visible in final states with two or three leptons. The $\gamma\gamma$ branching ratio is also strongly enhanced, so that in this case $hh \to WW\gamma\gamma$ also seems a promising final state. In particular, the request of one lepton from the decay of the W pair should be sufficient to reduce the background and lead to a clean signature at the LHC.

Figure 4 illustrates how the branching ratios $BR(hh \to \gamma\gamma b\bar{b})$ and $BR(hh \to WW\gamma\gamma)$ vary with c/a. Strong enhancements compared to the SM prediction are possible for $BR(hh \to WW\gamma\gamma)$ in the fermiophobic limit $c \to 0$. A fermiophobic composite Higgs can for example arise in the MCHM5 for $\xi \to 1/2$, see eq. (2.7). Although the point $(a = 1, c = 0)$ has been excluded at 95% CL in the range $m_h = 110 - 192\,\text{GeV}$ by the combination of all CMS searches [54], the one predicted by the MCHM5 for $\xi = 1/2$ $(a = 1/\sqrt{2}, c = 0)$ is still allowed for $m_h \sim 125\,\text{GeV}$ and in fact could better explain the pattern of observed enhancements in the various $\gamma\gamma$ categories of the CMS analysis [55]. Figure 5 shows the final yield per fb^{-1} predicted in the MCHM5 in the two final states $hh \to \gamma\gamma b\bar{b}$ and $hh \to WW\gamma\gamma \to l\nu q\bar{q}\gamma\gamma$ as a function of ξ for $m_h = 120\,\text{GeV}$. The rate has been computed using the cross section for $gg \to hh$ at LO in α_s (i.e. no K-factor is included) given by eq. (3.4) and table 1. As expected, for small values of ξ the most

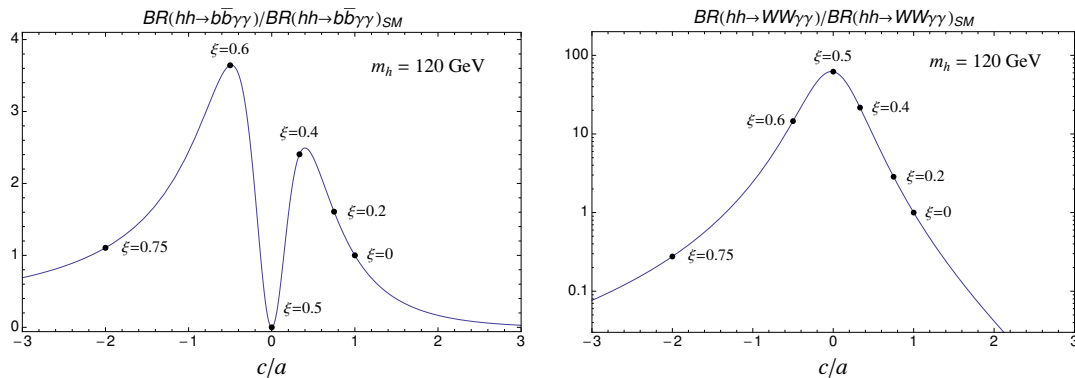**Figure 4**. Value of the branching ratio $BR(hh \to \gamma\gamma b\bar{b})$ (on the left) and $BR(hh \to WW\gamma\gamma)$ (on the right) in SM units as a function of the ratio of Higgs couplings c/a. The dots show the prediction in the MCHM5, where $c/a = (1-2\xi)/(1-\xi)$, for various values of ξ. In both plots the Higgs mass is set to $m_h = 120\,\text{GeV}$.
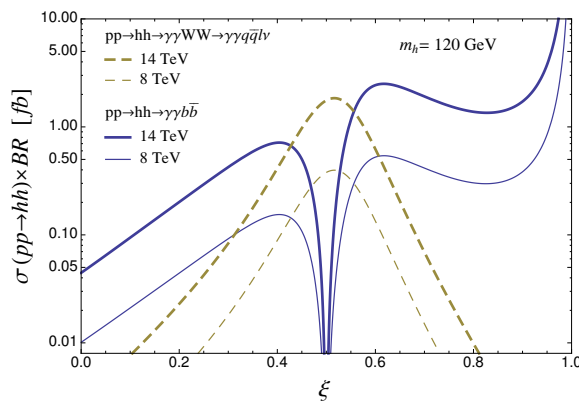

Figure 5. Signal yield per fb^{-1} predicted in the MCHM5 for the two final states $hh \to \gamma\gamma b\bar{b}$ (solid curves) and $hh \to WW\gamma\gamma \to l\nu q\bar{q}\gamma\gamma$ (dashed curves) as a function of ξ. The thick (thin) curves correspond to the LHC with $14\,\text{TeV}$ ($8\,\text{TeV}$) center-of-mass energy. The Higgs mass is set to $m_h = 120\,\text{GeV}$. The rate has been computed using the cross section for $gg \to hh$ at LO in α_s (i.e. no K-factor is included) given by eq. (3.4) and table 1.

promising channel is $\gamma\gamma b\bar{b}$, whose rate can be significantly enhanced compared to the SM expectation. At $14\,\text{TeV}$, for example, even for $\xi = 0.1$ the signal yield more than doubles. This large sensitivity to small values of $\xi = (v/f)^2$ shows that double Higgs production via gluon fusion is an extremely powerful process to probe the Higgs compositeness at the LHC. Still, the difficulty of isolating the $\gamma\gamma b\bar{b}$ signal from the background will require large integrated luminosities and will be possible only in the high-energy phase of the LHC. In the fortunate situation in which the Higgs is fermiophobic, on the other hand, the enhancement of the $hh \to WW\gamma\gamma \to l\nu q\bar{q}\gamma\gamma$ final state is so large in the MCHM5 that a first preliminary observation of the signal might be possible at the $8\,\text{TeV}$ LHC. At this energy, for $\xi = 1/2$, $m_h = 120\,\text{GeV}$ and $20\,\text{fb}^{-1}$ of integrated luminosity the MCHM5 predicts ~ 15 signal events before cuts.[2] Considering that the SM background is expected

---

[2]We included a K-factor $= 2$ in the estimate, which is the value obtained in ref. [28] at $14\,\text{TeV}$, assuming

to be rather small for a final state with two photons and one isolated lepton, this number of events might be sufficient to establish the observation of the signal. For the same value of c.o.m. energy and integrated luminosity, the MCHM5 predicts ~ 42 and ~ 27 signal events (before cuts) respectively in $hh \to 4W \to l^\pm l^\pm \nu\nu 4q$ (two same-sign leptons) and $hh \to 4W \to 3l3\nu q\bar{q}$. These high rates suggest that it might be possible to distinguish the $hh \to 4W$ signal over the SM background even at 8 TeV.

The results discussed in this section are rather encouraging, and show that double Higgs production can be an important process to extract or constrain the $t\bar{t}hh$ interaction and, more in general, to probe the Higgs compositeness. However, a more robust assessment of the LHC sensitivity in this sense requires a dedicated analysis of each of the relevant final states and a careful estimate of the background. In the next section we will focus on the $\gamma\gamma b\bar{b}$ channel and use the studies of ref. [32] to get a first determination of the precision which can be obtained on c_2 at the 14 TeV LHC.

4 Analysis of the $b\bar{b}\gamma\gamma$ channel

The analysis of the $gg \to hh \to b\bar{b}\gamma\gamma$ process performed in ref. [32] aimed at measuring the Higgs trilinear coupling, and assumed SM values for the other couplings. In this section we make use of the results of [32] to estimate the LHC sensitivity on the $t\bar{t}hh$ non-linear interaction.

We assume a center-of-mass energy $\sqrt{s} = 14$ TeV and set $m_h = 120$ GeV. Given the value of the signal rate and the large SM background, an analysis of $b\bar{b}\gamma\gamma$ at 8 TeV seems rather challenging and for this reason it will not be considered here. We expect our results at 14 TeV to be representative of what the LHC sensitivity will be in its future high-energy phase, even if the actual value of c.o.m. energy turns out to be different (on the prospects of 14 and 13 TeV see for example [56]). The analysis is performed at the parton level: signal events are generated by means of our implementation of double Higgs production via gluon fusion in ALPGEN, while the computation of the background processes is taken from [32]. We take the NLO QCD corrections to $gg \to hh$ into account by multiplying the LO cross section by a factor $K = 2$ [28],[3] while we neglect the smaller contribution of the vector-boson-fusion process to double Higgs production. To ensure an effective suppression of the background, we select events with two photons and two b-jets. Two photon tags are necessary to suppress the huge QCD background. On the other hand, the optimal number of b-tags depends on the strength of the signal and on the collider energy. In ref. [32] only one b-tag was required for the analysis at the 14 TeV LHC. This choice was motivated by the necessity of preserving the small SM signal as much as possible, at the expense of having to cope with a larger background. In our case the signal cross section is much larger than the SM one in a sizable part of the parameter space. Furthermore, recent studies have shown that a larger b-tagging efficiency than that assumed in ref. [32] is possible at the LHC [57, 58], maintaining an acceptable rejection rate on jets. In particular,

---

that a similar result also applies at 8 TeV. For $m_h = 125$ GeV the number of signal event is ~ 10.

[3] Notice that the authors of ref. [32] used a factor $K = 1.65$ for the LHC at 14 TeV, which is the one appropriate for their choice of the renormalization and factorization scale $Q = m_h$. As previously discussed, we set instead $Q = m(hh)$.

we adopt the following conservative estimates for the efficiencies (ϵ) and fake rates (r) for b-tagging [57, 58] and photon reconstruction [59]:[4]

$$\epsilon_\gamma = 0.8\,, \qquad r_\gamma = 2500\,, \qquad \epsilon_b = 0.7\,, \qquad r_{c\to b} = 5\,, \qquad r_{j\to b} = 25\,. \qquad (4.1)$$

This allows us to require two b-tags, thus obtaining a stronger suppression of the background at the price of an affordable reduction of the signal. We find that including the additional category of events with one b-tag in the analysis does not sensibly improve our results.

Following [32], we impose the set of kinematic cuts

$$p_T(b) > 45 \text{ GeV}\,, \qquad |\eta(b)| < 2.5\,, \qquad \Delta R(b,b) > 0.4\,,$$
$$m_h - 20 \text{ GeV} < m(b\bar{b}) < m_h + 20 \text{ GeV}\,,$$
$$p_T(\gamma) > 20 \text{ GeV}\,, \qquad |\eta(\gamma)| < 2.5\,, \qquad \Delta R(\gamma,\gamma) > 0.4\,, \qquad (4.2)$$
$$m_h - 2.3 \text{ GeV} < m(\gamma\gamma) < m_h + 2.3 \text{ GeV}\,,$$
$$\Delta R(\gamma,b) > 0.4\,,$$

which have a high selection efficiency on the signal and ensure that the $b\bar{b}$ and $\gamma\gamma$ invariant masses are reconstructed in the given windows around the Higgs mass. To take into account the detector resolution, we have assumed a 79% efficiency for the reconstruction of the $b\bar{b}$ pair and a 79% efficiency for the reconstruction of the $\gamma\gamma$ pair in the signal, as done in ref. [32]. After the above cuts, the most important irreducible backgrounds come from the $b\bar{b}\gamma\gamma$ continuum, and potentially by single Higgs production in association with two b-quarks ($h(\to \gamma\gamma)b\bar{b}$) or two photons ($h(\to b\bar{b})\gamma\gamma$). The reducible backgrounds are QCD processes ($c\bar{c}\gamma\gamma$, $b\bar{b}\gamma j$, $c\bar{c}\gamma j$, $b\bar{b}jj$, $c\bar{c}jj$, $\gamma\gamma jj$, γjjj, $jjjj$) or single-Higgs production processes (hjj and $hj\gamma$) where some of the jets fake one or more b-quarks or photons. While the QCD backgrounds are universal and as such are not affected by New Physics, those coming from single Higgs production depend on the value of the modified Higgs couplings. In the SM, all single Higgs processes are much smaller than the double Higgs signal after the cuts of eq. (4.2), and can be safely neglected [32]. This approximation is still valid in our context, and for this reason we will not include these backgrounds in our analysis. The list of relevant processes and their cross sections after the cuts of eq. (4.2) (without including b and photon reconstruction efficiencies) is reported in table 2.

A further suppression of the background can be obtained by exploiting the particular topology of the signal, where the two Higgs bosons are produced back to back in the center-of-mass frame. We thus select events where the $\gamma\gamma$ pair has a small opening angle, while the minimal angular separation between a b-jet and a photon is large. We require [32]:

$$\Delta R(\gamma,b) > 1.0\,, \qquad \Delta R(\gamma,\gamma) < 2.0\,. \qquad (4.3)$$

In most of the parameter space these cuts imply a moderate reduction of the signal ($20\% - 40\%$), while the total background is suppressed by one order of magnitude. The corresponding background cross sections are reported in the second line of table 2.

---

[4]The authors of ref. [32] use instead $\epsilon_b = 0.5$ and fake rates $r_{c\to b} = 13$ and $r_{j\to b} = 140$.

used cuts	$b\bar{b}\gamma\gamma$	$c\bar{c}\gamma\gamma$	$b\bar{b}\gamma j$	$c\bar{c}\gamma j$	$jj\gamma\gamma$	$b\bar{b}jj$	$c\bar{c}jj$	γjjj	$jjjj$
eq. (4.2)	0.056	0.42	65	250	11	2.5×10^{4}	2.5×10^{4}	7700	5×10^{6}
+ eq. (4.3)	0.0060	0.0215	8.28	17.0	0.84	4520	4520	364	4×10^{5}
+ tags	0.0019	5×10^{-4}	0.0013	2×10^{-4}	9×10^{-4}	4×10^{-4}	3×10^{-5}	2×10^{-4}	1×10^{-4}

Table 2. Cross sections (in fb) of the main QCD backgrounds to $hh \to b\bar{b}\gamma\gamma$ at the 14 TeV LHC. The values of the cross sections after the cuts of eqs. (4.2) and (4.3) are taken from [32], and include an additional rescaling factor 1.3 introduced to take into account the increase that can possibly come from NLO corrections. The last line reports the value of the cross sections after the inclusion of the b-jet and photon tagging efficiencies of eq. (4.1).

Finally, the reducible backgrounds are drastically suppressed once the efficiencies for reconstructing two photons and two b-jets of eq. (4.1) are included. The resulting final cross sections are shown in the last line of table 2. The corresponding total background cross section is $r_b = 5.5$ ab.

After performing the kinematic cuts of eqs. (4.2), (4.3) and including the efficiencies for the reconstruction of the $\gamma\gamma$ and $b\bar{b}$ pairs, the tagging efficiencies (4.1), and the K-factor, the signal rate ($r_s \equiv \sigma(pp \to hh) \times BR(hh \to \gamma\gamma b\bar{b})$) at $m_h = 120$ GeV is well approximated by the formula

$$r_s = \frac{BR(hh \to \gamma\gamma b\bar{b})}{BR(hh \to \gamma\gamma b\bar{b})_{SM}} \times (49.3\,\text{ab})\Big[c_2^2 + \left(0.407\,c^2\right)^2 + \left(0.101\,cd_3\right)^2 - 1.76\,c_2\left(0.407\,c^2\right)$$
$$- 1.82\left(0.407\,c^2\right)\left(0.101\,cd_3\right) + 1.72\,c_2\left(0.101\,cd_3\right)\Big].$$
$$(4.4)$$

For the SM case ($c = d_3 = 1$, $c_2 = 0$) we find $r_s = 4.9$ ab. Notice that, compared to the fit of eq. (3.4) at 14 TeV (see table 1), the cuts have further weakened the dependence of the cross section on d_3, since their efficiency is smaller for events with low $m(hh)$ invariant mass.

4.1 Results

Using the signal and background rates derived above, we can estimate the sensitivity of the 14 TeV LHC on $pp \to hh \to b\bar{b}\gamma\gamma$ for $m_h = 120$ GeV. Since large luminosities are typically needed to distinguish the signal from SM background, we expect that by the time the analysis of double Higgs production is performed, the Higgs branching ratios to $\gamma\gamma$ and $b\bar{b}$ and the linear couplings a, c are known with good accuracy. Double Higgs production can thus be used to extract (or set limits on) the couplings c_2 and d_3.

Figure 6 shows the luminosity required to discover the signal as a function of c, c_2 and d_3, assuming that the branching ratio $BR(hh \to \gamma\gamma b\bar{b})$ has the value predicted in the SM.[5] The plots on the left and on the right show the luminosity contours respectively in the plane (c_2, d_3) for $c = 1$, and in the plane (c, c_2) for $d_3 = c$. As expected, the sensitivity on c and c_2 is stronger than that on the Higgs trilinear coupling d_3. In particular, while a

---

[5]The definition of discovery luminosity and the details of our statistical analysis are discussed in the appendix.
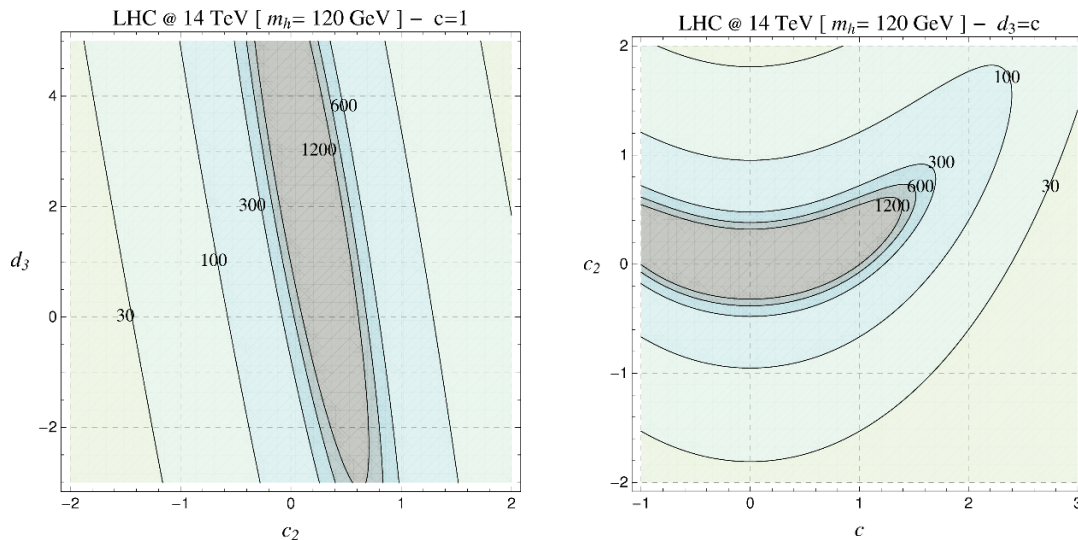
Figure 6. Isocurves of discovery luminosity (in fb^{-1}) at the 14 TeV LHC in the plane (c_2, d_3) for $c = 1$ (on the left) and in the plane (c, c_2) for $d_3 = c$ (on the right). Outside each contour, the $pp \to hh \to \gamma\gamma b\bar{b}$ signal can be discovered with the corresponding integrated luminosity. In both plots the Higgs mass is set to $m_h = 120$ GeV and the Higgs decay branching ratios are fixed to their SM values. See the appendix for the definition of discovery luminosity.
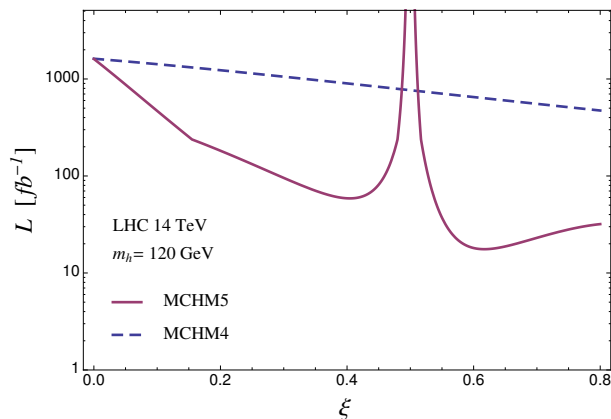
Figure 7. Discovery luminosity at the 14 TeV LHC in the MCHM4 (dashed blue curve) and MCHM5 (continuous purple curve) as a function of ξ. The Higgs mass is set to $m_h = 120$ GeV. See the appendix for the definition of discovery luminosity.

discovery in the SM would require at least 1200 fb^{-1}, we find that much lower luminosities are sufficient even for moderately small values of c_2. Figure 7 shows the corresponding discovery luminosity in the composite Higgs models MCHM4 and MCHM5 as a function of ξ. We find that values of ξ as small as 0.15 can be probed with 300 fb^{-1} of integrated luminosity. Compared to other processes like double Higgs production via vector boson fusion [39], these results show that $gg \to hh$ can be extremely powerful to study the non-linear couplings of a composite Higgs and thus probe its strong interactions.

Once a discovery is established, one can measure the couplings c_2 and d_3 by using the value of c and of the Higgs branching ratios determined in single-Higgs processes.
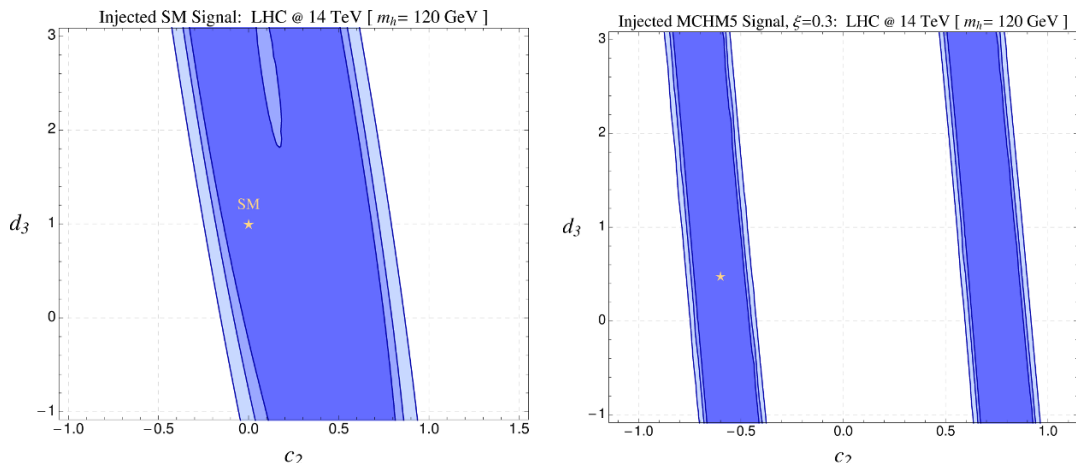
Figure 8. Regions of 68% probability in the plane (c_2, d_3) obtained with 300 (light blue area), 600 (medium dark blue area) and $1200\,\text{fb}^{-1}$ (darker blue area) of integrated luminosity. On the left: injected signal is the SM ($c = d_3 = 1$, $c_2 = 0$); On the right: injected signal is the MCHM5 with $\xi = 0.3$ ($c = d_3 = 0.48$, $c_2 = -0.6$). Both plots are obtained by assuming that the branching fraction $BR(hh \to \gamma\gamma b\bar{b})$ and the coupling c have been measured from single-Higgs processes with a 20% uncertainty.

The left plot of figure 8 shows the region of 68% probability in the plane (c_2, d_3) with 300, 600 and $1200\,\text{fb}^{-1}$ (light, medium and dark blue regions) obtained by injecting the SM signal ($c = d_3 = 1$, $c_2 = 0$) and assuming that the coupling c and the branching fraction $BR(hh \to \gamma\gamma b\bar{b})$ have been determined with a 20% accuracy.[6] In this case the precision on c_2 is poor even with $1200\,\text{fb}^{-1}$, while d_3 is basically unconstrained. A more precise determination of c_2 can be obtained if its value is non-vanishing. The right plot of figure 8 shows the case in which the injected signal is that of the MCHM5 with $\xi = 0.3$, corresponding to ($c = d_3 = 0.48$, $c_2 = -0.6$). It assumes that the branching fraction $BR(hh \to \gamma\gamma b\bar{b})$ and the coupling $c = 0.48$ predicted by this model have been measured with 20% accuracy in single-Higgs processes. We find that with $300\,\text{fb}^{-1}$ the coupling c_2 can be determined, up to a discrete ambiguity, with a precision of $\sim 20 - 30\%$.[7] On the other hand, even in this case d_3 remains largely unconstrained with our analysis. Finally, figure 9 shows how precisely the parameter ξ can be determined in the MCHM5 through $gg \to hh \to \gamma\gamma b\bar{b}$ by making use only of the value of the decay branching ratios determined in single-Higgs processes (that is: without fixing c to its measured value in the fit). As before, we assume that the branching fraction $BR(hh \to \gamma\gamma b\bar{b})$ is known with an error of 20%.

For each injected value ξ_{th}, the solid, dashed and dot-dashed curves (red, orange and yellow regions) show the 68% probability interval which is expected on the measured value ξ_{exp} respectively with 600, 300 and $100\,\text{fb}^{-1}$. For example, with $300\,\text{fb}^{-1}$ of integrated luminosity, $\xi = 0.2$ can be measured with a precision of $\sim 45\%$. The solid, dashed and

---

[6]That is: the rate of observed events is assumed to be that predicted in the SM with $m_h = 120\,\text{GeV}$. The uncertainties on c and $BR(hh \to \gamma\gamma b\bar{b})$ have been taken into account by marginalizing the 2-dimensional likelihood over two nuisance parameters, see appendix.

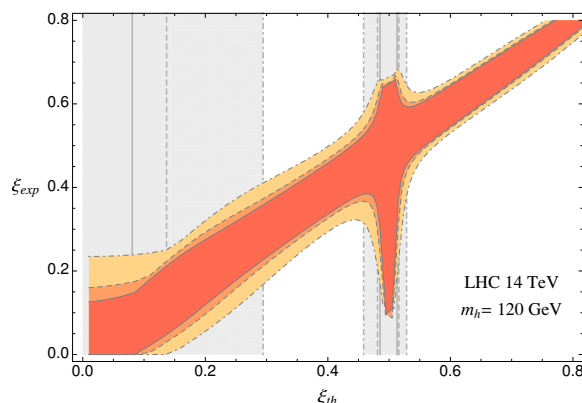[7]This improves to $\sim 15 - 20\%$ if the uncertainty on c and $BR(hh \to \gamma\gamma b\bar{b})$ is negligible.

Figure 9. Precision on the parameter ξ in the MCHM5 which can be obtained at the 14 TeV LHC for $m_h = 120$ GeV from the analysis of $pp \to hh \to \gamma\gamma b\bar{b}$. For each injected value ξ_{th}, the solid, dashed and dot-dashed curves (red, orange and yellow regions) show the 68% probability interval which is expected on the measured value ξ_{exp} respectively with 600, 300 and 100 fb^{-1}. The gray regions delimited by the solid, dashed and dot-dashed vertical lines indicate the values of ξ, respectively with 600, 300 and 100 fb^{-1}, for which the signal rate is too small to make a discovery, (see figure 7). In particular, for $\xi \to 0.5$ the $h \to b\bar{b}$ decay rate vanishes (the Higgs becomes fermiophobic), and the signal cannot be distinguished from the SM background. The curves are derived by assuming that the branching fraction $BR(hh \to \gamma\gamma b\bar{b})$ is determined with 20% accuracy from single-Higgs production.

dot-dashed vertical lines indicate the range of ξ, respectively for 600, 300 and 100 fb^{-1}, for which the expected signal yield is sufficiently large to establish a discovery (see figure 7).

5   Conclusions

The discovery of a light Higgs-like scalar at the LHC will mark a first important step forward in our comprehension of the electroweak symmetry breaking mechanism. Precise knowledge of the strength of its interactions with SM fields can shed light on the origin of the Higgs boson and indicate if the new dynamics at the electroweak scale is weakly or strongly interacting. New strong dynamics can form the Higgs as a bound state and solve naturally the hierarchy problem of the Standard Model. In this case the Higgs boson itself interacts strongly at large energies due to its modified linear couplings to SM fields and the existence of new non-linear interactions.

In this paper we have performed a first model-independent study of double Higgs production via gluon fusion, $gg \to hh$, and we have shown that its cross section is greatly enhanced by the non-linear interaction $t\bar{t}hh$. Such new vertex gives a contribution to the scattering amplitude of $t\bar{t} \to hh$ that grows with the energy, $\mathcal{A}(t\bar{t} \to hh) \sim (Em_t)/v^2$, and as such it is a genuine signature of the underlying strong dynamics. In the process $gg \to hh$ the $t\bar{t}hh$ vertex mediates a new diagram containing a top-quark loop which grows logarithmically at high energies and does not lead to a violation of perturbative unitarity (see eq. (3.3)). However, it does lead to a strong numerical enhancement of the cross section compared to the SM, as first noticed by the authors of ref. [35] in the context of

the MCHM composite Higgs models. The origin of this enhancement can in part be traced back to the sizable destructive interference which occurs in the Standard Model between the box and the triangle diagram with Higgs exchange. A similar cancellation has been found to take place at large $\hat{s}$ in $gg \to ZZ$ [60] and $gg \to WW$ [62], and interpreted as a relic of the cancellation dictated by unitarity between the energy-growing amplitudes in the sub-process $t\bar{t} \to VV$. On the other hand, in the case of double Higgs production the cancellation is in the *total* cross section (i.e. not necessarily at large $\hat{s}$). Furthermore, none of the diagrams which contribute to $t\bar{t} \to hh$ in the SM grows with the energy, so that the cancellation between the box and the triangle diagram in $gg \to hh$ should be rather seen as a numerical accident, not driven by the unitarity of its subprocess.

The strong enhancement of the $gg \to hh$ cross section makes this process quite powerful to measure or constrain the strength of the $t\bar{t}hh$ interaction, which we have denoted as c_2. This should be compared with the much weaker sensitivity on the Higgs trilinear interaction, d_3, which makes the extraction of this latter coupling extremely challenging at the LHC. In particular, the weaker dependence on d_3 follows from an extra suppressing factor $(m_h^2/\hat{s})$ carried by the triangle diagram with Higgs exchange, which thus contributes mainly at threshold. In order to assess the LHC precision on c_2 we have made use of the results of refs. [29–32], where double Higgs production via gluon fusion was studied in the context of the SM and several Higgs decay channels were investigated. In a generic scenario of New Physics, what is the best final state largely depends on the value of the Higgs decay branching ratios. In particular, enhanced branching ratios can combine with the increase in the double Higgs production cross section and lead to dramatic effects at the LHC. For example, in the (fermiophobic) limit in which the linear couplings of the Higgs to the SM fermions are suppressed ($c \to 0$), the $h \to WW$ and $h \to \gamma\gamma$ branching ratios can be sensibly enhanced compared to their SM values. In this case the final states $hh \to WWWW$ and $hh \to WW\gamma\gamma$ seem to be extremely promising, and might be visible even at the 8 TeV LHC. At this energy and with $L = 20\,\mathrm{fb}^{-1}$, for example, we find that for $m_h = 120\,\mathrm{GeV}$ the MCHM5 at $\xi = 0.5$ predicts ~ 15 signal events in $hh \to WW\gamma\gamma \to l\nu q\bar{q}\gamma\gamma$ (see figure 5).

If the Higgs decay branching ratios do not differ much from their SM values and the Higgs boson is light, the most powerful final state should be $hh \to b\bar{b}\gamma\gamma$, as suggested by the analysis of ref. [32]. Even in this case, the signal rate can be significantly enhanced compared to the SM prediction if c_2 is not too small. At 14 TeV, for example, the signal rate predicted in the MCHM5 with $\xi = 0.1$ is larger than the SM one by more than a factor two. This sensitivity on small values of $\xi = (v/f)^2$ shows that double Higgs production via gluon fusion is an extremely powerful process to probe the Higgs compositeness at the LHC. In order to estimate the LHC sensitivity on c_2 in a model-independent way, we have followed the strategy proposed in ref. [32] and performed a MonteCarlo study of $pp \to hh \to b\bar{b}\gamma\gamma$. We have computed the SM background cross section by using the results reported in [32] and rescaling them to take account of updated b and γ efficiencies and rejection factors. The results that we obtained are quite encouraging. With $L = 300\,\mathrm{fb}^{-1}$ the 14 TeV LHC can probe values $c_2 \lesssim -0.2$ and $c_2 \gtrsim 0.8$ if $c, d_3 \sim 1$ (see figure 6). In the case of the MCHM5, an integrated luminosity of $300\,\mathrm{fb}^{-1}$ is sufficient to discover a signal with $\xi \gtrsim 0.15$ (see figure 7). In general, once the signal can be statistically distinguished

from the background and a discovery is made, the value of c_2 can be extracted with good accuracy. For example, we find that by injecting a signal with $c = d_3 = 0.48$ and $c_2 = -0.6$ (as predicted in the MCHM5 for $\xi = 0.3$), the coupling c_2 can be measured, up to a discrete ambiguity, with a precision of $\sim 20 - 30\%$ (see figure 8).

Our partonic analysis of $pp \to hh \to b\bar{b}\gamma\gamma$ should be considered as a first estimate of the LHC potentiality, although we expect it to be robust and moderately conservative. For example, we have followed a cut-based strategy to reduce the background, although a realistic analysis will certainly make use of shape variables and extract the background from data, similarly to what has been done by the ATLAS and CMS collaborations in single Higgs searches. Also notice that we did not make use of the information on the total invariant mass distribution, $d\sigma/dm(b\bar{b}\gamma\gamma)$, which was instead used in ref. [32] to further increase the signal significance. Finally, a more precise assessment of the LHC sensitivity will require full inclusion of showering and hadronization effects, as well as a detector simulation.

Acknowledgments

A Details of the statistical analysis

We report here the details of the statistical analysis used to derive our results. We follow the Bayesian approach[8] and construct a posterior probability for the total event rate r,

$$p_{\mathcal{L}}(r|N) \propto L(N|r\mathcal{L})\,\pi(r) \tag{A.1}$$

for given number of observed events N and luminosity $\mathcal{L}$. We denote with $\pi(r)$ the prior distribution and with $L(N|r\mathcal{L})$ the likelihood function, which we take to be a Poisson distribution

$$L(N|r\mathcal{L}) = \frac{e^{-r\mathcal{L}}\,(r\mathcal{L})^N}{N!}\,. \tag{A.2}$$

For the plots of figures 6, 7 we use a prior distribution which is flat for $r > 0$ and vanishing otherwise, and normalize the probability so that $\int_0^\infty dr\, p_{\mathcal{L}}(r|N) = 1$. The discovery contours of figures 6 and 7 are obtained by setting the number of observed events to the

---

[8]See for example ref. [63] for a primer.

total value $N = (r_s + r_b)\mathcal{L}$ expected in each point of the Higgs couplings' parameter space: $r_s = r_s(a, c, c_2, d_3)$ for figure 6, $r_s = r_s(\xi)$ for figure 7. We define a point in this space to be 'discoverable' at a certain luminosity $\mathcal{L}$ if the probability of having a total number of events smaller than or equal to $r_b\mathcal{L}$ is below 1%,

$$\int_0^{r_b} dr' \, p_{\mathcal{L}}(r' | (r_s + r_b)\mathcal{L}) \leq 0.01 \,, \tag{A.3}$$

and if the number of observed events $(r_s + r_b)\mathcal{L}$ is 5 or larger. The discovery luminosity is thus defined to be the smallest value of $\mathcal{L}$ which satisfies these two conditions.

In the case of the plot of figure 8, we marginalize the probability function over all possible values of the coupling c and of the branching fraction $BR(hh \to \gamma\gamma b\bar{b})$ assuming that they have a Gaussian distribution around their central value with 20% relative error. In practice, we set

$$r_s(c_2, d_3, \theta_1, \theta_2) \equiv (1 + \delta_1\theta_1) \, BR(hh \to \gamma\gamma b\bar{b}) \, \sigma(\bar{c}(1 + \delta_2\theta_2), c_2, d_3) \,, \tag{A.4}$$

where $\sigma(c, c_2, d_3)$ is the signal production cross section, $\delta_{1,2} = 0.20$ and $\bar{c}$ denotes the central value of c, and integrate over the nuisance parameters $\theta_{1,2}$:

$$p_{\mathcal{L}}(c_2, d_3 | N) \propto \int d\theta_1 \int d\theta_2 \, e^{-\theta_1^2/2} e^{-\theta_2^2/2} \, L(N | (r_s(c_2, d_3, \theta_1, \theta_2) + r_b)\mathcal{L}) \, \pi(c_2, d_3) \,. \tag{A.5}$$

The prior distribution is assumed to be flat over the plane (c_2, d_3) and the posterior probability is normalized so that $\int dc_2 \int dd_3 \, p_{\mathcal{L}}(c_2, d_3 | N) = 1$.

Finally, the plot of figure 9 has been derived by expressing the posterior probability as a function of ξ and marginalizing over all possible values of the branching fraction:

$$p_{\mathcal{L}}(\xi | N) \propto \int d\theta_1 \, e^{-\theta_1^2/2} \, L(N | ((1 + \delta_1\theta_1) \, r_s(\xi) + r_b)\mathcal{L}) \, \pi(\xi) \,. \tag{A.6}$$

We choose a flat prior for $0 \leq \xi \leq 1$ (vanishing otherwise) and normalize the probability so that $\int_0^1 d\xi \, p_{\mathcal{L}}(\xi | N) = 1$. For each value ξ_{th} the number of observed events has been set to the total expected value $N = (r_s(\xi_{\text{th}}) + r_b)\mathcal{L}$.

References

[1] D.B. Kaplan and H. Georgi, SU(2) × U(1) *breaking by vacuum misalignment*, *Phys. Lett.* **B 136** (1984) 183 [INSPIRE].

[2] S. Dimopoulos and J. Preskill, *Massless composites with massive constituents*, *Nucl. Phys.* **B 199** (1982) 206 [INSPIRE].

[3] T. Banks, *Constraints on* SU(2) × U(1) *breaking by vacuum misalignment*, *Nucl. Phys.* **B 243** (1984) 125 [INSPIRE].

[4] D.B. Kaplan, H. Georgi and S. Dimopoulos, *Composite Higgs scalars*, *Phys. Lett.* **B 136** (1984) 187 [INSPIRE].

[5] H. Georgi, D.B. Kaplan and P. Galison, *Calculation of the composite Higgs mass*, *Phys. Lett.* **B 143** (1984) 152 [INSPIRE].

[6] H. Georgi and D.B. Kaplan, *Composite Higgs and custodial* SU(2), *Phys. Lett.* **B 145** (1984) 216 [INSPIRE].

[7] M.J. Dugan, H. Georgi and D.B. Kaplan, *Anatomy of a composite Higgs model*, *Nucl. Phys.* **B 254** (1985) 299 [INSPIRE].

[8] D. Zeppenfeld, R. Kinnunen, A. Nikitenko and E. Richter-Was, *Measuring Higgs boson couplings at the CERN LHC*, *Phys. Rev.* **D 62** (2000) 013009 [hep-ph/0002036] [INSPIRE].

[9] PRECISION HIGGS WORKING GROUP OF SNOWMASS 2001 collaboration, J. Conway, K. Desch, J. Gunion, S. Mrenna and D. Zeppenfeld, *The precision of Higgs boson measurements and their implications*, *eConf* **C 010630** (2001) P1WG2 [hep-ph/0203206] [INSPIRE].

[10] A. Belyaev and L. Reina, $pp \to t\bar{t}H, H \to \tau^+\tau^-$: *toward a model independent determination of the Higgs boson couplings at the LHC*, *JHEP* **08** (2002) 041 [hep-ph/0205270] [INSPIRE].

[11] M. Duhrssen, *Prospects for the measurement of Higgs boson coupling parameters in the mass range from* 110–190 *GeV*, ATL-PHYS-2003-030 (2003).

[12] M. Dührssen et al., *Extracting Higgs boson couplings from CERN LHC data*, *Phys. Rev.* **D 70** (2004) 113009 [hep-ph/0406323] [INSPIRE].

[13] R. Lafaye, T. Plehn, M. Rauch, D. Zerwas and M. Dührssen, *Measuring the Higgs sector*, *JHEP* **08** (2009) 009 [arXiv:0904.3866] [INSPIRE].

[14] S. Bock et al., *Measuring hidden Higgs and strongly-interacting Higgs scenarios*, *Phys. Lett.* **B 694** (2010) 44 [arXiv:1007.2645] [INSPIRE].

[15] F. Bonnet, M. Gavela, T. Ota and W. Winter, *Anomalous Higgs couplings at the LHC and their theoretical interpretation*, *Phys. Rev.* **D 85** (2012) 035016 [arXiv:1105.5140] [INSPIRE].

[16] D. Carmi, A. Falkowski, E. Kuflik and T. Volansky, *Interpreting LHC Higgs results from natural new physics perspective*, *JHEP* **07** (2012) 136 [arXiv:1202.3144] [INSPIRE].

[17] A. Azatov, R. Contino and J. Galloway, *Model-independent bounds on a light Higgs*, *JHEP* **04** (2012) 127 [arXiv:1202.3415] [INSPIRE].

[18] J. Espinosa, C. Grojean, M. Muhlleitner and M. Trott, *Fingerprinting Higgs suspects at the LHC*, *JHEP* **05** (2012) 097 [arXiv:1202.3697] [INSPIRE].

[19] P.P. Giardino, K. Kannike, M. Raidal and A. Strumia, *Reconstructing Higgs boson properties from the LHC and Tevatron data*, *JHEP* **06** (2012) 117 [arXiv:1203.4254] [INSPIRE].

[20] M. Rauch, *Determination of Higgs-boson couplings (SFitter)*, arXiv:1203.6826 [INSPIRE].

[21] J. Ellis and T. You, *Global analysis of experimental constraints on a possible Higgs-like particle with mass* $\sim$ 125 *GeV*, *JHEP* **06** (2012) 140 [arXiv:1204.0464] [INSPIRE].

[22] A. Azatov et al., *Determining Higgs couplings with a model-independent analysis of* $h \to \gamma\gamma$, *JHEP* **06** (2012) 134 [arXiv:1204.4817] [INSPIRE].

[23] M. Farina, C. Grojean and E. Salvioni, *(Dys)Zphilia or a custodial breaking Higgs at the LHC*, *JHEP* **07** (2012) 012 [arXiv:1205.0011] [INSPIRE].

[24] C. Degrande, J. Gerard, C. Grojean, F. Maltoni and G. Servant, *Probing top-Higgs non-standard interactions at the LHC*, *JHEP* **07** (2012) 036 [arXiv:1205.1065] [INSPIRE].

[25] M. Klute, R. Lafaye, T. Plehn, M. Rauch and D. Zerwas, *Measuring Higgs couplings from LHC data*, arXiv:1205.2699 [INSPIRE].

[26] E.N. Glover and J.J. van der Bij, *Higgs boson pair production via gluon fusion*, *Nucl. Phys.* **B 309** (1988) 282 [INSPIRE].

[27] T. Plehn, M. Spira and P. Zerwas, *Pair production of neutral Higgs particles in gluon-gluon collisions*, *Nucl. Phys.* **B 479** (1996) 46 [*Erratum ibid.* **B 531** (1998) 655] [hep-ph/9603205] [INSPIRE].

[28] S. Dawson, S. Dittmaier and M. Spira, *Neutral Higgs boson pair production at hadron colliders: QCD corrections*, *Phys. Rev.* **D 58** (1998) 115012 [hep-ph/9805244] [INSPIRE].

[29] U. Baur, T. Plehn and D.L. Rainwater, *Measuring the Higgs boson self coupling at the LHC and finite top mass matrix elements*, *Phys. Rev. Lett.* **89** (2002) 151801 [hep-ph/0206024] [INSPIRE].

[30] U. Baur, T. Plehn and D.L. Rainwater, *Determining the Higgs boson selfcoupling at hadron colliders*, *Phys. Rev.* **D 67** (2003) 033003 [hep-ph/0211224] [INSPIRE].

[31] U. Baur, T. Plehn and D.L. Rainwater, *Examining the Higgs boson potential at lepton and hadron colliders: a comparative analysis*, *Phys. Rev.* **D 68** (2003) 033001 [hep-ph/0304015] [INSPIRE].

[32] U. Baur, T. Plehn and D.L. Rainwater, *Probing the Higgs selfcoupling at hadron colliders using rare decays*, *Phys. Rev.* **D 69** (2004) 053004 [hep-ph/0310056] [INSPIRE].

[33] K. Agashe, R. Contino and A. Pomarol, *The minimal composite Higgs model*, *Nucl. Phys.* **B 719** (2005) 165 [hep-ph/0412089] [INSPIRE].

[34] R. Contino, L. Da Rold and A. Pomarol, *Light custodians in natural composite Higgs models*, *Phys. Rev.* **D 75** (2007) 055014 [hep-ph/0612048] [INSPIRE].

[35] R. Grober and M. Muhlleitner, *Composite Higgs boson pair production at the LHC*, *JHEP* **06** (2011) 020 [arXiv:1012.1562] [INSPIRE].

[36] C.O. Dib, R. Rosenfeld and A. Zerwekh, *Double Higgs production and quadratic divergence cancellation in little Higgs models with T parity*, *JHEP* **05** (2006) 074 [hep-ph/0509179] [INSPIRE].

[37] M. Moretti, S. Moretti, F. Piccinini, R. Pittau and A. Polosa, *Higgs boson self-couplings at the LHC as a probe of extended Higgs sectors*, *JHEP* **02** (2005) 024 [hep-ph/0410334] [INSPIRE].

[38] G. Giudice, C. Grojean, A. Pomarol and R. Rattazzi, *The strongly-interacting light Higgs*, *JHEP* **06** (2007) 045 [hep-ph/0703164] [INSPIRE].

[39] R. Contino, C. Grojean, M. Moretti, F. Piccinini and R. Rattazzi, *Strong double Higgs production at the LHC*, *JHEP* **05** (2010) 089 [arXiv:1002.1011] [INSPIRE].

[40] R. Contino, D. Marzocca, D. Pappadopulo and R. Rattazzi, *On the effect of resonances in composite Higgs phenomenology*, *JHEP* **10** (2011) 081 [arXiv:1109.1570] [INSPIRE].

[41] M.L. Mangano, M. Moretti, F. Piccinini, R. Pittau and A.D. Polosa, *ALPGEN, a generator for hard multiparton processes in hadronic collisions*, *JHEP* **07** (2003) 001 [hep-ph/0206293] [INSPIRE].

[42] A. Pierce, J. Thaler and L.-T. Wang, *Disentangling dimension six operators through di-Higgs boson production*, *JHEP* **05** (2007) 070 [hep-ph/0609049] [INSPIRE].

[43] I. Low, R. Rattazzi and A. Vichi, *Theoretical constraints on the Higgs effective couplings*, *JHEP* **04** (2010) 126 [arXiv:0907.5413] [INSPIRE].

[44] A. Azatov and J. Galloway, *Light custodians and Higgs physics in composite models*, *Phys. Rev.* **D 85** (2012) 055013 [`arXiv:1110.5646`] [InSPIRE].

[45] A. Falkowski, *Pseudo-goldstone Higgs production via gluon fusion*, *Phys. Rev.* **D 77** (2008) 055018 [`arXiv:0711.0828`] [InSPIRE].

[46] E. Furlan, *Gluon-fusion Higgs production at NNLO for a non-standard Higgs sector*, *JHEP* **10** (2011) 115 [`arXiv:1106.4024`] [InSPIRE].

[47] G. Panico and A. Wulzer, *The discrete composite Higgs model*, *JHEP* **09** (2011) 135 [`arXiv:1106.2719`] [InSPIRE].

[48] S. De Curtis, M. Redi and A. Tesi, *The 4D composite Higgs*, *JHEP* **04** (2012) 042 [`arXiv:1110.1613`] [InSPIRE].

[49] O. Matsedonskyi, G. Panico and A. Wulzer, *Light top partners for a light composite Higgs*, `arXiv:1204.6333` [InSPIRE].

[50] M. Redi and A. Tesi, *Implications of a light Higgs in composite models*, `arXiv:1205.0232` [InSPIRE].

[51] D. Marzocca, M. Serone and J. Shu, *General composite Higgs models*, *JHEP* **08** (2012) 013 [`arXiv:1205.0770`] [InSPIRE].

[52] R.K. Ellis and G. Zanderighi, *Scalar one-loop integrals for QCD*, *JHEP* **02** (2008) 002 [`arXiv:0712.1851`] [InSPIRE].

[53] M. Whalley, D. Bourilkov and R. Group, *The Les Houches accord PDFs (LHAPDF) and LHAGLUE*, `hep-ph/0508110` [InSPIRE].

[54] CMS collaboration, *Combined results of searches for a Higgs boson in the context of the standard model and beyond-standard models*, CMS-PAS-HIG-12-008 (2012).

[55] CMS collaboration, *Search for the fermiophobic model Higgs boson decaying into two photons*, CMS-PAS-HIG-12-002 (2012).

[56] E. Todesco, C. Lorin and M. Bajko, *Energy of the LHC after the 2013–2014 shutdown*, in *LHC Performance Workshop (Chamonix 2012)*, February 6–10, Chamonix, France (2012).

[57] ATLAS collaboration, *Measurement of the b-tag efficiency in a sample of jets containing muons with $5\,fb^{-1}$ of data from the ATLAS detector*, ATLAS-CONF-2012-043 (2012).

[58] CMS collaboration, *b-Jet Identification in the CMS Experiment*, PAS-BTV-11-004 (2011).

[59] ATLAS collaboration, *Expected photon performance in the ATLAS experiment*, PHYS-PUB-2011-007 (2011).

[60] E.N. Glover and J. van der Bij, *Vector boson pair production via gluon fusion*, *Phys. Lett.* **B 219** (1989) 488 [InSPIRE].

[61] E.N. Glover and J. van der Bij, *Z boson pair production via gluon fusion*, *Nucl. Phys.* **B 321** (1989) 561 [InSPIRE].

[62] E. Accomando, *The process $gg \to WW$ as a probe into the EWSB mechanism*, *Phys. Lett.* **B 661** (2008) 129 [`arXiv:0709.1364`] [InSPIRE].

[63] G. D'Agostini, *Bayesian reasoning in data analysis: a critical introduction*, World Scientific, Singapore (2003).